

pubs.acs.org/NanoLett Letter

# Enhanced Cycling Stability of All-Solid-State Lithium—Sulfur Battery through Nonconductive Polar Hosts

Tianwei Jin, Keyue Liang, Jeong-Hoon Yu, Ting Wang, Yihan Li, Tai-De Li, Shyue Ping Ong, Jong-Sung Yu,\* and Yuan Yang\*



Cite This: Nano Lett. 2024, 24, 6625-6633



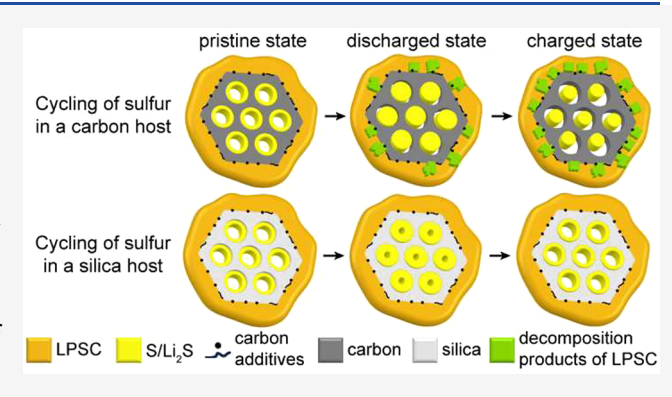
**ACCESS** I

III Metrics & More

Article Recommendations

s Supporting Information

ABSTRACT: All-solid-state lithium—sulfur batteries (ASSLSBs) are promising next-generation battery technologies with a high energy density and excellent safety. Because of the insulating nature of sulfur/Li<sub>2</sub>S, conventional cathode designs focus on developing porous hosts with high electronic conductivities such as porous carbon. However, carbon hosts boost the decomposition of sulfide electrolytes and suffer from sulfur detachment due to their weak bonding with sulfur/Li<sub>2</sub>S, resulting in capacity decays. Herein, we propose a counterintuitive design concept of host materials in which nonconductive polar mesoporous hosts can enhance the cycling life of ASSLSBs through mitigating the decomposition of adjacent electrolytes and bonding sulfur/Li<sub>2</sub>S steadily to avoid detachment. By using a mesoporous SiO<sub>2</sub> host filled with 70 wt %



sulfur as the cathode, we demonstrate steady cycling in ASSLSBs with a capacity reversibility of 95.1% in the initial cycle and a discharge capacity of 1446 mAh/g after 500 cycles at C/5 based on the mass of sulfur.

KEYWORDS: all-solid-state lithium—sulfur batteries, nonconductive hosts, polarity, silica, sulfur detachment

ithium-sulfur batteries (LSBs) have attracted substantial Lattention as a promising next-generation energy storage solution due to the ultrahigh specific capacity, high natural abundance, and environment friendliness of sulfur. 1-3 However, the development of LSBs with liquid electrolytes is hindered by several key challenges. First, organic solvents in LSBs, which are highly flammable, dissolve intermediate lithium polysulfides, and the consequent shuttle effect results in low Coulombic efficiencies (CE) and short lifespan.<sup>4</sup> Second, the electrically and ionically insulating nature of sulfur and Li<sub>2</sub>S leads to sluggish cathode kinetics. Third, the large volume change of ~80% from sulfur to Li<sub>2</sub>S causes them to lose contact with carbon additives and electrolytes, resulting in a substantial capacity loss.<sup>6,7</sup> Recently, all-solid-state lithiumsulfur batteries (ASSLSBs) have attracted increasing attention as a potential solution.<sup>8,9</sup> By adopting inorganic sulfide solidstate electrolytes (SSEs), such as Li<sub>6</sub>PS<sub>5</sub>Cl (LPSC) and Li<sub>10</sub>GeP<sub>2</sub>S<sub>12</sub> (LGPS) with high ionic conductivities (10<sup>-3</sup>– 10<sup>-2</sup> S cm<sup>-1</sup>) and favorable mechanical properties, the shuttle effect can be eliminated together with greatly elevated battery safety. 10-12

To enhance the reaction kinetics in LSBs, high-surface-area conductive carbon hosts are often used. 13,14 Unfortunately, sulfide electrolytes in ASSLSBs usually have narrow electrochemical stability windows, and Meng et al. have revealed that the oxidation and reduction decomposition of sulfides will be

accelerated when they are exposed to electronic conductors. <sup>15–17</sup> Therefore, though nanoporous carbon hosts enhance the electron transfer to sulfur, their high electronic conductivities could also boost the decomposition of adjacent sulfide SSEs into insulating components (Figure 1a), which consequently impede the ion transport for the S/Li<sub>2</sub>S redox. <sup>18</sup> As a result, the cathode kinetics deteriorates over successive cycles and cell capacities accordingly diminish. <sup>19,20</sup> Alternatively, various nanoporous oxides are nonconductive so that they are expected to suppress the decomposition of neighboring SSEs and retain the cycling stability, and the electronic conduction could be fulfilled by other strategies, such as reduced sulfur sizes and proper carbon additives with low specific surface areas (Figure 1b).

The other potential advantage of oxides over carbon as hosts for sulfur is their strong bonding with active materials. Carbon hosts have weak bonding with sulfur and Li<sub>2</sub>S due to its nonpolarity, and previous works showed the active material would detach from the carbon hosts upon volume expansion

Received: March 11, 2024 Revised: May 21, 2024 Accepted: May 22, 2024 Published: May 24, 2024





Nano Letters pubs.acs.org/NanoLett Letter

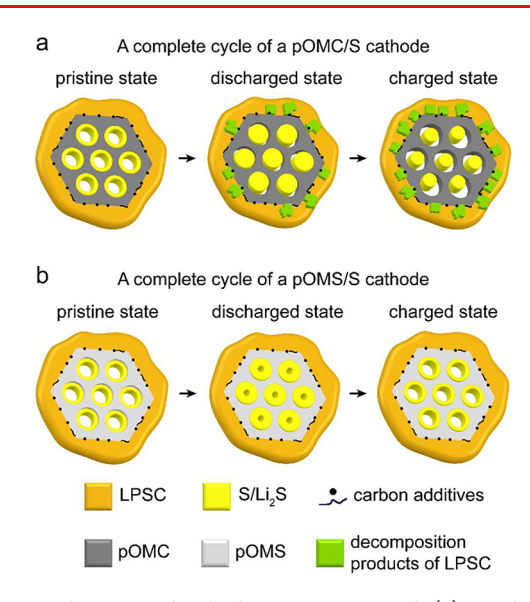


**Figure 1.** Schematics of cathodes in ASSLSBs with (a) a carbon host (platelet ordered mesoporous carbon, pOMC) and (b) a nonconductive polar host (platelet ordered mesoporous silica, pOMS), respectively. The highly conductive carbon host promotes the decomposition of adjacent electrolytes, and sulfur filled in the carbon host suffers from the detachment issue during cycling. In contrast, the polar silica host bonds strongly to the active materials, and its low electronic conductivity accordingly suppresses the electrolyte decomposition.

and contraction (Figure 1a), leading to loss in conduction pathway and capacity. <sup>21–24</sup> In contrast, oxides are found to have strong chemisorption toward lithium sulfides out of their high polarities, making them good candidates as sulfur hosts or separator coatings in the LSBs with liquid electrolytes to mitigate the shuttle effect. <sup>25–32</sup> Such superior bindings indicate that oxide hosts could potentially solve the sulfur detaching issue in carbon hosts and allow ASSLSBs to achieve better cycling performance.

Based on these hypotheses, herein, we propose a counterintuitive concept that nonconductive polar hosts can substantially enhance the performance of ASSLSBs. As a demonstration, we synthesized a platelet ordered mesoporous silica (pOMS, Figure 1b) and a platelet ordered mesoporous carbon (pOMC, Figure 1a) as model systems for insulating oxide hosts and conductive carbon hosts, respectively. The platelet-shaped OMS and OMC feature structural advantages over conventional rod-like ones, such as much shorter mesopore nanochannels for homogeneous sulfur loading and shorter pathways for ions and electrons during cycling.<sup>33</sup>

The pOMS/S composite with 70 wt % sulfur showed an excellent cycling performance, which presented a capacity reversibility of 95.1% in the initial cycle and delivered a steady discharge capacity of 1446 mAh/g after 500 cycles at C/5 at room temperature. In contrast, the pOMC/S composite with 70 wt % sulfur showed a poor capacity reversibility of 75.7% in the initial cycle, probably due to electrolyte decomposition and sulfur detachment, with a fast capacity decay from 1430 mAh/g in cycle 1 to 649 mAh/g in cycle 50 at C/10 at room temperature. Further postcycling characterizations based on FIB-EDS mapping and XPS revealed that the insulating SiO<sub>2</sub> host significantly suppresses solid electrolyte decomposition and enhances sulfur/host binding. With all of those findings, this work unveiled an unexpected strategy to accelerate the

ASSLSB development to achieve high-energy-density lithium batteries

To study the effects of nonconductive polar hosts in ASSLSBs, pOMC and pOMS particles with similar morphology and pore structures were synthesized via a precipitation method based on our previous reports. 26,34 Sulfur then infiltrated into the open mesopore nanochannels of the hosts by sulfur vapor deposition in a weight ratio of 70:30 (sulfur:host), named as pOMC/S70 and pOMS/S70. As scanning electron microscopy (SEM) images showed, pOMC/ S70 (Figure 2a) and pOMS/S70 (Figure 2e) both have a thin hexagonal prism morphology with a thickness of ~250 nm and an edge length of 500-1000 nm. Transmission electron microscopy (TEM) images showed the open mesopores through the prism thickness of pOMC/S70 (Figure 2b) and pOMS/S70 (Figure 2f), and the corresponding high-angle annular dark-field scanning transmission electron microscopy (HAADF-STEM) element mapping images confirmed the uniform sulfur infusion in pOMC/S70 (Figure 2c,d) and pOMS/S70 (Figure 2g,h).

X-ray diffraction (XRD) patterns in Figure 2i further showed that pOMC and pOMS were amorphous, <sup>35,36</sup> and sulfur was amorphous or partially crystalline in pOMC/S70 and pOMS/S70. In addition, small-angle XRD results of pOMS (Figure S1a) and pOMC (Figure S1b) indicated the presence of a strong (100) and two weak (110) and (200) diffraction peaks, verifying a 2D hexagonal p6mm pore structure.<sup>37</sup> The corresponding spacing between pores is ~9.8 nm in both pOMS and pOMC. The diminishment of the (100), (110), and (200) peaks after the sulfur infusion denoted that sulfur indeed infiltrated into the pores.

In terms of pore structures, Brunauer–Emmett–Teller (BET) analysis (Figure 2j) showed that pOMC and pOMS have specific surface areas of 1643 and 864 m²/g, respectively. The corresponding pore size distributions centered at 4.2 nm for pOMC and 7.3 nm for pOMS, respectively (Figure S2). After loading with sulfur, the surface area of pOMC/S70 and pOMS/S70 sharply decreased to 45 and 15 m²/g (Figure 2j), respectively, with very low pore volumes (Figure S2), consistent with XRD confirmation. In addition, the 70 wt % sulfur loading was confirmed by thermogravimetric analysis (TGA) in Figure S3, a high value that is needed to increase the energy density of ASSLSBs.

Though pOMS/S70 and pOMC/S70 present similar physical properties, they behave chemically distinctly in terms of the sulfur interaction, as revealed by X-ray photoelectron spectroscopy (XPS). pOMC/S70 displayed almost the identical S 2p spectrum as elemental sulfur, deconvoluted into a spin—orbit doublet (S  $2p_{1/2}$  at 164.9~eV and  $2p_{3/2}$  at 163.7~eV) with an intensity ratio of 1:2 (Figure 2k), indicating no or weak interaction between sulfur and the carbon host.  $^{38}$  In contrast, the S 2p spectrum of pOMS/S70 in Figure 2l was remarkedly different, and the new peaks at 163.2 and 164.4~eV were identified to be Si–S bond,  $^{39,40}$  and such interaction with sulfur was also observed in other polysulfide trapping hosts.  $^{41,42}$ 

To elucidate the interfacial interactions between sulfur/Li<sub>2</sub>S and the host, density functional theory (DFT) calculations were performed. In Figure 2m, the calculated adhesion energy for the C–Li<sub>2</sub>S interface is -0.25 J/m<sup>2</sup> with a negligible interaction tendency observed at the interface. Conversely, the adhesion energy for the SiO<sub>2</sub>–Li<sub>2</sub>S interface is -0.93 J/m<sup>2</sup> with Si–S and Li–O distances of 0.22 and 0.20 nm,

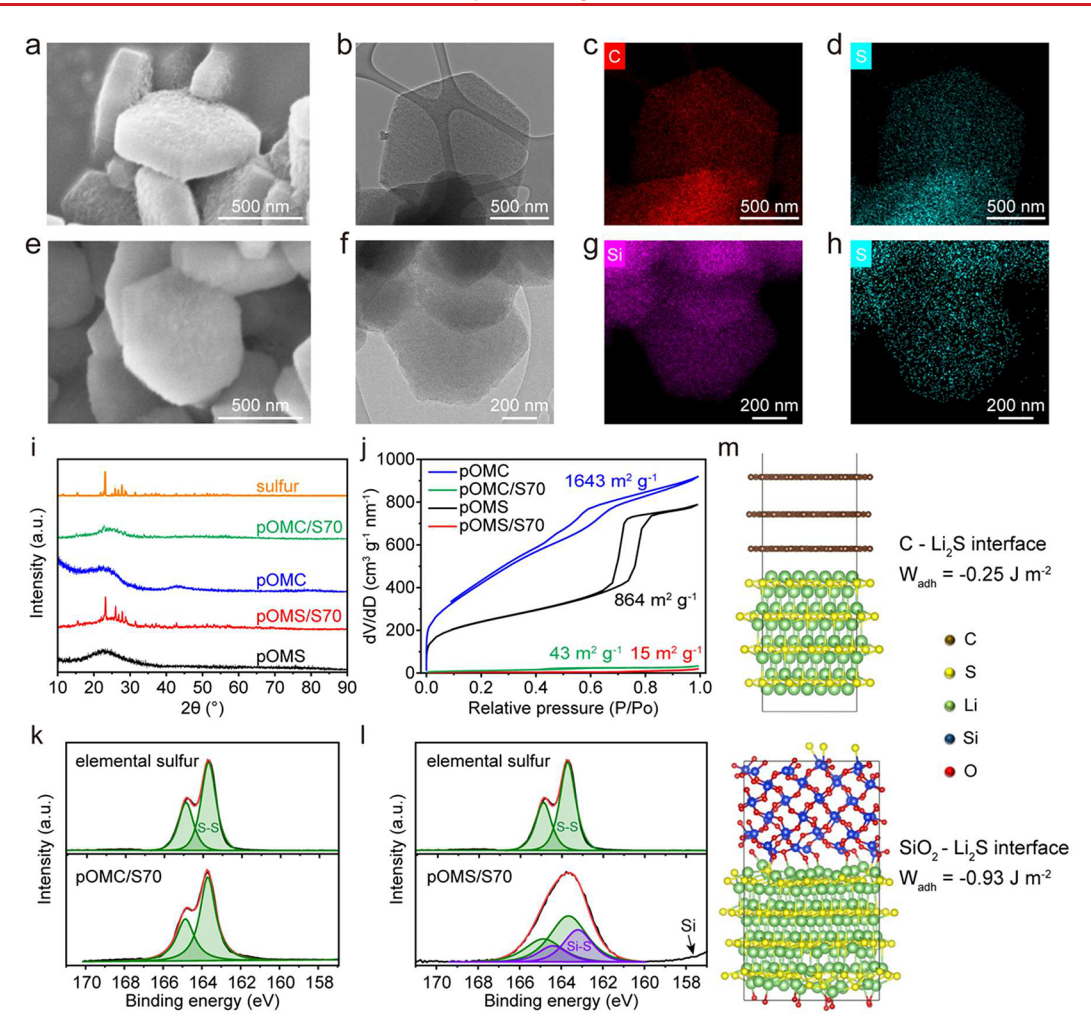


Figure 2. Physical and chemical properties of pOMS and pOMC hosts. (a–d) pOMC/S70: (a) SEM image, (b) TEM image, and (c, d) corresponding HAAD-STEM element mapping of (c) C and (d) S. (e–h) pOMS/S70: (e) SEM image, (f) TEM image, (g, h) corresponding HAAD-STEM element mapping of (g) Si and (h) S. (i) XRD patterns of elemental sulfur, pOMC, pOMC/S70, pOMS, and pOMS/S70. (j) Nitrogen adsorption/desorption isothermal profiles of pOMC, pOMC/S70, pOMS, and pOMS/S70. (k, l) Deconvoluted high-resolution S 2p XPS spectra of (k) pOMC/S70 and (l) pOMS/S70 with elemental sulfur as the reference. (m) DFT calculation of the interface structures of SiO<sub>2</sub>–Li<sub>2</sub>S and C–Li<sub>2</sub>S.

respectively, indicating strong interaction and even bond formation. The distinct adhesion energies are in consistent with prior reports that  $\text{Li}_2\text{S}$  bonds weakly with carbon but strongly with silica, thereby implying the potential of silica hosts to mitigate sulfur detachment issues observed with carbon hosts.  $^{22,25,26,43}$ 

Regarding interactions with sulfur (Figure S4), the adhesion energy for the C–S interface is determined to be 9.15 J/m². This positive and high value indicates a significant challenge for sulfur wetting on the carbon surface. On the other hand, the adhesion energy for the  $\mathrm{SiO}_2$ –S interface is only  $0.50\,\mathrm{J/m}^2$ . Although it remains positive, the significantly lower value suggests that sulfur exhibits a much stronger affinity for  $\mathrm{SiO}_2$  than for carbon. These DFT calculations suggest that silica hosts are capable of better fixing sulfur and  $\mathrm{Li}_2\mathrm{S}$  spatially to facilitate their robust contacts with SSEs and carbon additives during volume changes, thus enhancing the sulfur utilization and cycling stability of ASSLSBs relative to carbon hosts.

The discrepancy between the positive adhesion energy value for the  $SiO_2$ –S contact in the DFT calculation and the XPS result, indicating a strong Si–S bond, may be attributed to the presence of defects, such as oxygen vacancies, in silica. These

defects in practical scenarios, particularly on the surface, could facilitate the formation of Si–S bonds. However, in DFT calculations, interfaces are typically modeled between perfect materials at 0 K without any vacancies, which does not favor bond formation and can account for the positive adhesion energy value.

To illustrate the impact of polarity and nonconductivity of sulfur hosts on the electrochemical performances in ASSLSBs, 40 wt % pOMS/S70 and pOMC/S70 were respectively mixed with 40 wt % LPSC and 20 wt % carbon additives (8 wt % C65 carbon black, 8 wt % vapor-grown carbon fiber, and 4 wt % carbon nanotube) to build cathodes. The integration of such three carbon additives provided a sufficient electronic conduction network with a limited surface area to reduce electrolyte decomposition. 15 The cathode was then paired with an LPSC electrolyte and an Li-In anode and cycled within 1.2–3.0 V vs Li/Li<sup>+</sup>. The corresponding cycling performance is displayed in Figure 3a, and the voltage profiles are shown in Figure 3b,c. Although pOMC/S70 exhibited a high specific capacity of 1430 mAh/g in the initial discharge at C/10 with 1C defined as 1000 mA/g for all cells, only 1082 mAh/g (75.7%) was recovered in the subsequent charge (Figure 3b).

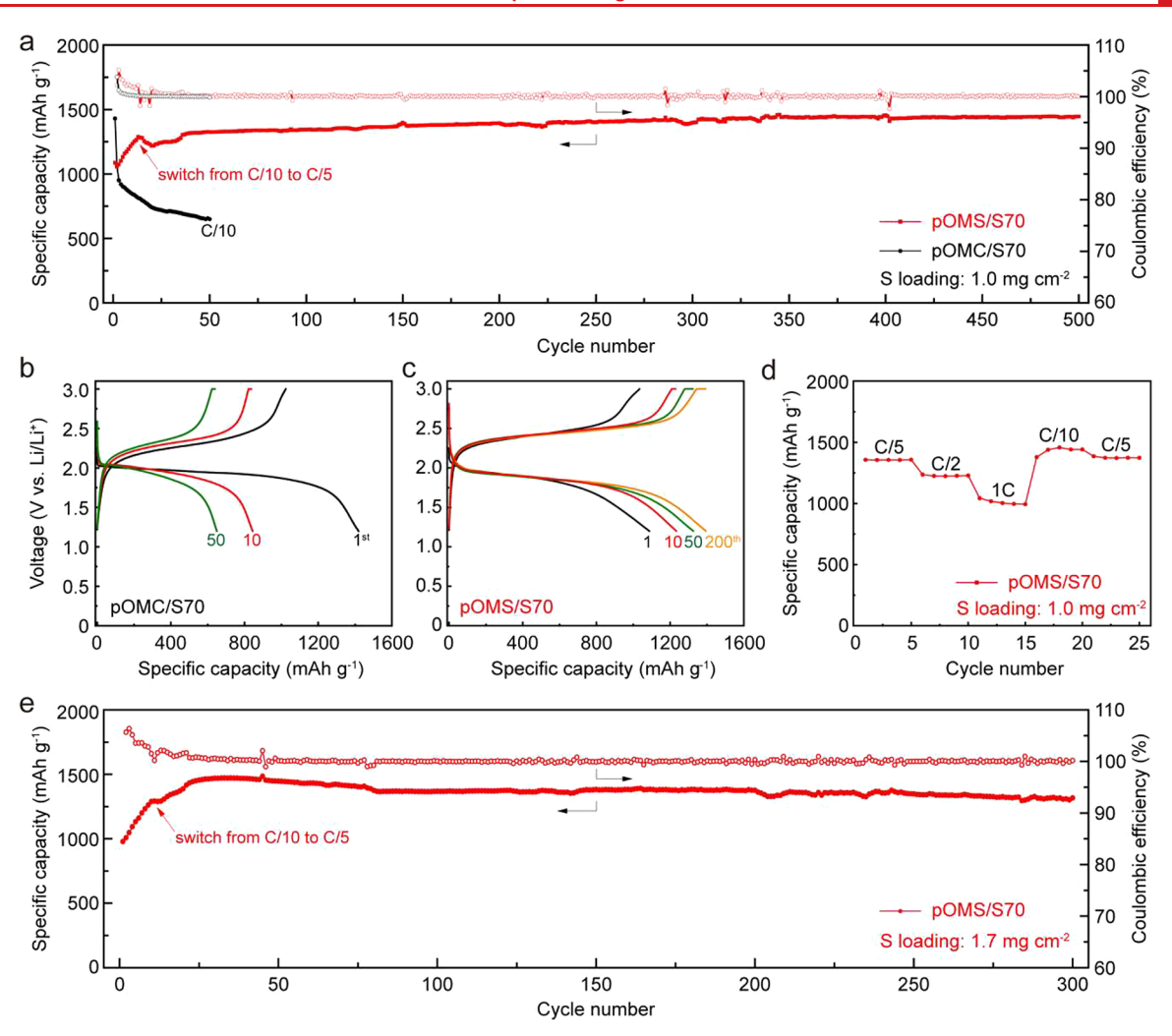


Figure 3. Electrochemical performance of all-solid-state Li—S batteries with a carbon host and a silica host, respectively. (a) Cycling performance of Li—InILPSClpOMS/S70 and Li—InILPSClpOMC/S70 cells with a mass loading of 1 mg/cm² sulfur and (b, c) their corresponding voltage profiles for (b) pOMC/S70 and (c) pOMS/S70. (d) Rate performance of a Li—InILPSClpOMS/S70 cell after 150 cycles (see Figure S6 for the full cycling performance). (e) Cycling performance of a Li—InILPSClpOMS/S70 cell with a higher mass loading of 1.7 mg/cm² sulfur. All cells underwent an initial cycle at C/20, followed by subsequent cycles at C/10 or C/5 with a constant-voltage step with a current cutoff of C/20. 1C is defined as 1000 mA/g for all cells based on the average specific capacity in the first cycle. All of the cells were cycled at room temperature.

Such a low reversibility could be caused by the electrolyte decomposition and sulfur detachment from the nonpolar carbon host, leading to a low sulfur utilization in the following cycles.<sup>21</sup>

In contrast, pOMS/S70 delivered a specific capacity of 1087 mAh/g in the initial discharge, and 1034 mAh/g was recovered in the subsequent charge (Figure 3c), corresponding to a reversibility of 95.1%. Such a high specific capacity also indicates that a conductive host is not the only option for ASSLSBs, and reasonable electronic transport can be achieved by a proper amount of carbon additives and reduced sulfur nanoparticle sizes to shorten the conducting pathway. As pOMS/S70 shares analogous morphological properties with pOMC/S70, the substantial enhancement in initial reversibility should not arise from morphological difference but could be attributed to the suppressed electrolyte decomposition and robust bonding of polar silica with sulfur/Li<sub>2</sub>S, ensuring well-preserved electronic and ionic conduction of sulfur.

In addition to the improved reversibility in the first cycle, pOMS/S70 also demonstrated significantly enhanced long-term cycling performance compared to that of pOMC/S70.

pOMS/S70 exhibited a distinct activation stage where the specific capacity substantially increased from 1087 mAh/g in the first cycle to 1318 mAh/g in the 40th cycle and to 1446 mAh/g in the 500th cycle at C/5, whose cycling stability is among the best results in reported ASSLSB works (Table S2). In contrast, the specific capacity of pOMC/S70 rapidly decreased from 1430 to 649 mAh/g after 50 cycles at C/10. Moreover, sulfur cathodes without nanoporous hosts showed markedly reduced specific capacities of less than 300 mAh/g (Figure S5), which arises from compromised kinetics and sulfur utilization due to a smaller contact area with LPSC/carbon and a longer transport pathway.<sup>20</sup>

We think that the gradual capacity increase in pOMS/S70 arose from the increasing contacts between S/Li<sub>2</sub>S and carbon additives/SSEs during volume expansion and contraction in cycling. Similar behaviors have also been reported in other works on ASSLSBs.  $^{44,45}$  Moreover, the insulating nature of SiO<sub>2</sub> also minimized the decomposition of sulfide electrolytes, and the strong bonding between S/Li<sub>2</sub>S and SiO<sub>2</sub> anchored the active materials to avoid detachment from the hosts and the loss of conducting contact. On the contrary, the sulfur

Nano Letters pubs.acs.org/NanoLett Letter

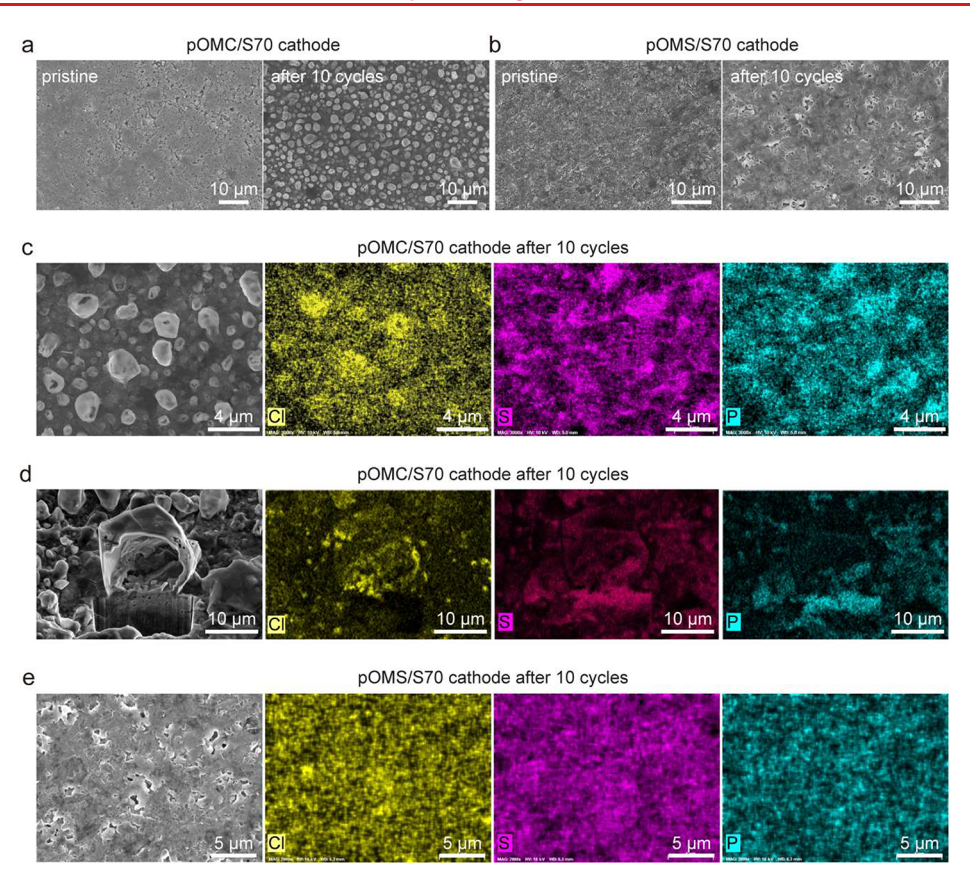


Figure 4. Morphological and chemical evolution of pOMS/S70 and pOMC/S70 cathodes. (a) SEM images of the pOMC/S70 cathode before and after 10 cycles. (b) SEM images of the pOMS/S70 cathode before and after 10 cycles. (c) SEM image of the pOMC/S70 cathode after 10 cycles and the corresponding EDS elemental mapping of Cl, S, and P. (d) FIB-SEM image of the pOMC/S70 cathode after 10 cycles and the corresponding EDS elemental mapping of Cl, S, and P. (e) SEM image of the pOMS/S70 cathode after 10 cycles and the corresponding EDS elemental mapping of Cl, S, and P. All cathodes after cycling were retrieved from all-solid-state cells at 3 V vs Li/Li<sup>+</sup> with a mass loading of 1 mg/cm<sup>2</sup> sulfur, cycled at C/20 for the first cycle and at C/10 for the following nine cycles at room temperature.

utilization in the carbon host would deteriorate at each cycle due to the decomposition of electrolyte and detachment from carbon, resulting in capacity decay.

Besides the steady long-term cycling performance, pOMS/S70 also exhibited satisfying rate performance at current rates from C/10 to 1 C (Figure 3d). pOMS/S70 exhibited an average discharge capacity of 1356 mAh/g at C/5, 1228 mAh/g at C/2, 1011 mAh/g at 1 C. The capacities recovered to 1431 mAh/g at C/10 and 1375 mAh/g at C/5, highlighting its outstanding rate performance and stability (see Figure S6 for the full cycling performance). It further validates that the electronic conduction can be satisfied in an insulating host with reduced sulfur sizes and a limited amount of carbon additives.

Based on all benefits of silica hosts shown above, we further demonstrated a long cycle life with a higher loading of 1.7 mg/cm² sulfur. As shown in Figure 3e, the cathode delivered a specific capacity of 978 mAh/g in the first cycle, which increased to 1467 mAh/g after 40 cycles and was maintained at 1317 mAh/g after 300 cycles with an average CE of 100.3%. To demonstrate the reproducibility of our proposed design, more Li–InlLPSClpOMS/S70 cells with similar cycling performance are shown in Figure S7. Cycling performance of a cathode with a higher sulfur content of 35 wt % is also demonstrated (Figure S8), illustrating that the cycling is still stable with higher sulfur contents thanks to the nonconductive polar host. All cycling results above show that nonconductive

polar sulfur hosts can enable the excellent performance of ASSLSBs.

It is worth mentioning that though nonconductive polar hosts could allow a better cycling life via suppressing SSE decomposition and sulfur detachment, the cathode kinetics was inferior to those with a conductive carbon host, as the voltage hysteresis of pOMS/S70 was larger than pOMC/S70 (0.59 V vs 0.36 V in the initial cycle, Figure 3b,c). It suggests that the host conductivity should be carefully designed to be moderate to simultaneously meet the criteria of both power capability and cycling life of ASSLSBs, which may also allow higher sulfur contents for high energy densities.

To elucidate the origin of the distinct electrochemical performance of pOMS/S70 and pOMC/S70 cathodes, SEM and energy dispersive spectroscopy (EDS) were employed to analyze their morphological and chemical changes after cycling. As shown in Figure 4a, numerous micrometer-sized agglomerates appeared in the pOMC/S70 cathode after 10 cycles, which was also reported in other ASSLSB studies. <sup>46</sup> Further EDS mapping elucidated that P signals overlapped well with S but complementary to Cl, whose signals concentrated in the agglomerate areas (Figure 4c). Such a separation of Cl from P and S agreed well with the previous studies that LPSC decomposes into LiCl, P<sub>2</sub>S<sub>5</sub>, Li<sub>2</sub>S, P during cycling, indicating a severe LPSC decomposition in the pOMC/S70 cathode after 10 cycles. <sup>17</sup> The fine structure of the agglomerates was further revealed by focused ion beam (FIB) milling. As shown in

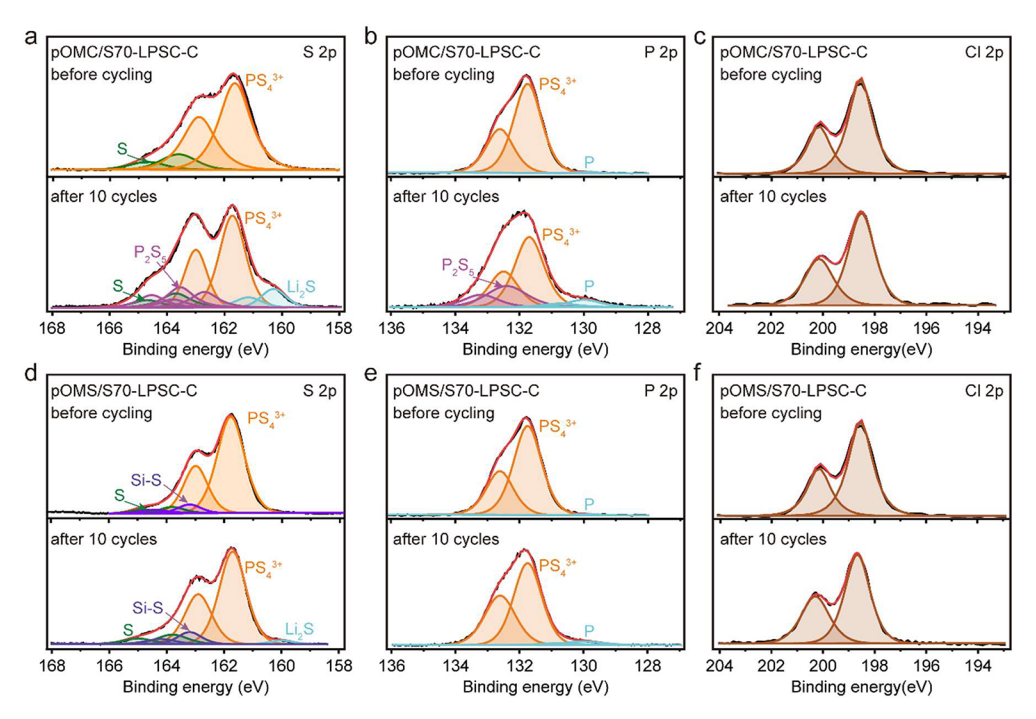


Figure 5. Deconvoluted high-resolution XPS spectra of the pOMS/S70 and pOMC/S70 cathodes. (a) S 2p, (b) P 2p, and (c) Cl 2p XPS spectra of the pOMC/S70 cathodes before and after 10 cycles. (d) S 2p, (e) P 2p, and (f) Cl 2p XPS spectra of the pOMS/S70 cathodes before and after 10 cycles. All cathodes after cycling were retrieved from all-solid-state cells at 3 V vs Li/Li<sup>+</sup> with a mass loading of 1 mg/cm<sup>2</sup> sulfur, cycled at C/20 for the first cycle and at C/10 for the following nine cycles at room temperature.

Figure 4d, the agglomerates had a shell structure with the EDS mapping of P overlapping with S but complementary to Cl, and scattered  $\sim\!\!1~\mu m$  Cl-rich domains were observed. Such results suggested that the LPSC decomposition, which would expand in volume, in the pOMC/S70 cathode might cause chemical redistribution, and the electronic and ionic conduction pathways of sulfur could be blocked when pOMC/S70 particles were surrounded by the insulating LiCl and  $P_2S_5^{-16,47}$ 

In contrast, LPSC decomposition was well alleviated in the pOMS/S70 cathode. As shown in Figure 4b, the morphology of the pOMS/S70 cathode remained intact after 10 cycles, and the corresponding EDS elemental mapping in Figure 4e also showed a uniform distribution of Cl, P, and S without separation, indicating that the LPSC remained essentially intact. The stable chemical distribution in the cathode ensured robust electronic and ionic conduction in the cathode and excellent electrochemical performance.

X-ray photoelectron spectroscopy (XPS) was further employed to elucidate chemical changes of cathodes in ASSLSBs. Figure 5a-c shows the XPS spectra of S, P, and Cl in pOMC/S70 cathodes before cycling and after 10 cycles. The S 2p spectrum of the pristine pOMC/S70 cathode had peaks at 161.8 and 163.70 eV with their spin-orbit doublets (S 2p<sub>1/2</sub> and 2p<sub>3/2</sub>), corresponding to the PS<sub>4</sub><sup>3+</sup> in LPSC electrolyte and elemental sulfur, respectively (Figure 5a). 38,48 However, a strong new peak at 160.1 eV with its spin-orbit doublet from Li<sub>2</sub>S and appreciable new peaks at 162.70 and 163.50 with their spin-orbit doublets from P<sub>2</sub>S<sub>5</sub> appeared at the charged state after 10 cycles, 48,49 which were from the irreversible lithiation of sulfur during cycles and LPSC decomposition.<sup>21</sup> The P 2p spectrum of the pristine pOMC/ S70 cathode had a peak at 131.70 eV with its spin-orbit doublet from the PS<sub>4</sub><sup>3+</sup> in LPSC and very weak elemental P

peak at 130.0 eV which came from the electrolyte impurity (Figure 5b). After 10 cycles, significant peaks at 132.40 eV from  $P_2S_5$  and 130.0 eV from P with their spin—orbit doublets were observed, which were the LPSC decomposition products. The Cl 2p spectrum had no change after 10 cycles because the Cl bonding energy in LPSC and LiCl were the same (Figure 5c).  $^{50}$ 

On the contrary, the LPSC degradation in pOMS/S70 cathodes after 10 cycles was significantly suppressed. As shown in Figure 5d, the S 2p spectrum of the pOMS/S70 cathode remained basically the same as the pristine state expect for a small peak of Li<sub>2</sub>S that might come from the irreversible lithiation of the sulfur during cycling. The P 2p spectrum in Figure 5e also showed that the only decomposition product was a small amount of elemental P at a much lower level than that of the pOMC/S70 cathode after cycling. The Cl 2p spectrum also remained the same as shown in Figure 5f.

Besides after 10 cycles, we further studied the XPS spectra of the pOMS/S70 cathode after 300 cycles (Figure S9), which showed that the electrolyte decomposition catalyzed by the carbon additives is substantially slower and less than the decomposition catalyzed by pOMC/S70. This indicates that an appreciable amount of the electrolyte decomposition in the pOMC/S70 cathode is caused by the carbon mesoporous hosts and thus is adjacent to S/Li<sub>2</sub>S, which will severely block the conduction pathway of Li<sup>+</sup> and e<sup>-</sup> to S/Li<sub>2</sub>S and lead to capacity decay. In contrast, decomposition from carbon additives (e.g., VGCF) is less and has a smaller impact on the conduction pathways. In summary, the XPS results above illustrated that the electrolyte decomposition was successfully restrained by using a nonconductive SiO<sub>2</sub> host compared to carbon hosts.

In conclusion, we innovatively proposed a new design concept for the sulfur hosts in ASSLSBs that low conductivities Nano Letters pubs.acs.org/NanoLett Letter

could suppress the adjacent electrolyte decomposition and high polarities could mitigate the sulfur detachment issue, thereby enhancing the cycling performance of ASSLSBs. The adequate electronic conduction of sulfur can be realized with reduced sulfur nanoparticle sizes and proper choices of carbon additives rather than merely replying on conductive hosts. Accordingly, a silica host for sulfur which has strong bonding with sulfur and Li<sub>2</sub>S was demonstrated. The SiO<sub>2</sub>/S composite delivered a discharge capacity of 1087 mAh/g in cycle 1, 95.1% of which was reversible in the following charging and 1446 mAh/g after 500 cycles at C/5. In contrast, C/S composite delivered a discharge specific capacity of 1430 mAh/g in cycle 1, 75.7% of which was reversible in the following charging, and only 649 mAh/g after 50 cycles at C/10. The excellent performance of the SiO<sub>2</sub>/S composite is attributed to reduced electrolyte decomposition and better attachment between SiO<sub>2</sub> and active materials, which are confirmed by FIB-SEM-EDS and XPS analysis. This study unveils that nonconductive polar hosts could be attractive for ASSLSBs because of the mitigated electrolyte decomposition, stabilized cycling, and satisfying power density.

### ASSOCIATED CONTENT

## Supporting Information

The Supporting Information is available free of charge at https://pubs.acs.org/doi/10.1021/acs.nanolett.4c01210.

Experimental section, additional figures of material characterizations, DFT calculations, and cycling performance (Figures S1–S9), and tables of DFT information and cycling performance comparison with literature (Tables S1 and S2) (PDF)

## AUTHOR INFORMATION

## **Corresponding Authors**

Jong-Sung Yu — Department of Energy Science and Engineering, Daegu Gyeongbuk Institute of Science and Technology, Daegu 42988, Republic of Korea; Energy Science and Engineering Research Center, Daegu Gyeongbuk Institute of Science and Technology, Daegu 42988, Republic of Korea; orcid.org/0000-0002-8805-012X; Email: jsyu@dgist.ac.kr

Yuan Yang — Program of Materials Science and Engineering, Department of Applied Physics and Applied Mathematics, Columbia University, New York, New York 10027, United States; orcid.org/0000-0003-0264-2640; Email: yy2664@columbia.edu

## Authors

Tianwei Jin — Program of Materials Science and Engineering, Department of Applied Physics and Applied Mathematics, Columbia University, New York, New York 10027, United States; oorcid.org/0000-0002-4355-5474

Keyue Liang — Program of Materials Science and Engineering, Department of Applied Physics and Applied Mathematics, Columbia University, New York, New York 10027, United

**Jeong-Hoon Yu** – Department of Energy Science and Engineering, Daegu Gyeongbuk Institute of Science and Technology, Daegu 42988, Republic of Korea

Ting Wang — Department of NanoEngineering, University of California, San Diego, La Jolla, California 92093-0448, United States

Yihan Li – Program of Materials Science and Engineering, Department of Applied Physics and Applied Mathematics, Columbia University, New York, New York 10027, United States

Tai-De Li — Nanoscience Initiative at Advanced Science Research Center, Graduate Center of the City University of New York, New York, New York 10031, United States; Department of Physics, City College of New York, City University of New York, New York, New York 10031, United States

Shyue Ping Ong – Department of NanoEngineering, University of California, San Diego, La Jolla, California 92093-0448, United States

Complete contact information is available at: https://pubs.acs.org/10.1021/acs.nanolett.4c01210

#### Notes

The authors declare no competing financial interest.

#### ACKNOWLEDGMENTS

The authors greatly appreciate the funding support from AFOSR (Grants FA9550-22-1-0226 and FA9550-23-1-0071) and Korea Research Foundation (Grant RS-2023-00223196) and valuable discussions with Xiao Sun at Northeastern University. The computational studies were supported by the National Science Foundation Materials Research Science and Engineering Center program through the UC Irvine Center for Complex and Active Materials (Grant DMR-2011967). The computation work used Expanse at San Diego Supercomputer Center through Allocation DMR150014 from the Advanced Cyberinfrastructure Coordination Ecosystem: Services & Support (ACCESS) program, which is supported by National Science Foundation Grants 2138259, 2138286, 2138307, 2137603, and 2138296.

#### REFERENCES

- (1) Pang, Q.; Liang, X.; Kwok, C. Y.; Nazar, L. F. Advances in lithium—sulfur batteries based on multifunctional cathodes and electrolytes. *Nat. Energy* **2016**, *1* (9), No. 16132.
- (2) Manthiram, A.; Fu, Y.; Chung, S.-H.; Zu, C.; Su, Y.-S. Rechargeable Lithium—Sulfur Batteries. *Chem. Rev.* **2014**, *114* (23), 11751—11787.
- (3) Yang, X.; Li, X.; Adair, K.; Zhang, H.; Sun, X. Structural Design of Lithium—Sulfur Batteries: From Fundamental Research to Practical Application. *Electrochemical Energy Reviews* **2018**, *1* (3), 239–293.
- (4) Lei, T.; Chen, W.; Lv, W.; Huang, J.; Zhu, J.; Chu, J.; Yan, C.; Wu, C.; Yan, Y.; He, W.; Xiong, J.; Li, Y.; Yan, C.; Goodenough, J. B.; Duan, X. Inhibiting Polysulfide Shuttling with a Graphene Composite Separator for Highly Robust Lithium-Sulfur Batteries. *Joule* 2018, 2 (10), 2091–2104.
- (5) Ye, H.; Li, M.; Liu, T.; Li, Y.; Lu, J. Activating Li2S as the Lithium-Containing Cathode in Lithium-Sulfur Batteries. *ACS Energy Letters* **2020**, 5 (7), 2234–2245.
- (6) Wei Seh, Z.; Li, W.; Cha, J. J.; Zheng, G.; Yang, Y.; McDowell, M. T.; Hsu, P.-C.; Cui, Y. Sulphur—TiO2 yolk—shell nanoarchitecture with internal void space for long-cycle lithium—sulphur batteries. *Nat. Commun.* **2013**, *4* (1), 1331.
- (7) Fu, K.; Gong, Y.; Hitz, G. T.; McOwen, D. W.; Li, Y.; Xu, S.; Wen, Y.; Zhang, L.; Wang, C.; Pastel, G.; Dai, J.; Liu, B.; Xie, H.; Yao, Y.; Wachsman, E. D.; Hu, L. Three-dimensional bilayer garnet solid electrolyte based high energy density lithium metal—sulfur batteries. *Energy Environ. Sci.* **2017**, *10* (7), 1568–1575.
- (8) Ding, B.; Wang, J.; Fan, Z.; Chen, S.; Lin, Q.; Lu, X.; Dou, H.; Kumar Nanjundan, A.; Yushin, G.; Zhang, X.; Yamauchi, Y. Solid-

- state lithium-sulfur batteries: Advances, challenges and perspectives. *Mater. Today* **2020**, *40*, 114–131.
- (9) Xu, R.; Yue, J.; Liu, S.; Tu, J.; Han, F.; Liu, P.; Wang, C. Cathode-Supported All-Solid-State Lithium—Sulfur Batteries with High Cell-Level Energy Density. ACS Energy Letters 2019, 4 (5), 1073—1079.
- (10) Park, K. H.; Bai, Q.; Kim, D. H.; Oh, D. Y.; Zhu, Y.; Mo, Y.; Jung, Y. S. Design Strategies, Practical Considerations, and New Solution Processes of Sulfide Solid Electrolytes for All-Solid-State Batteries. *Adv. Energy Mater.* **2018**, *8* (18), No. 1800035.
- (11) Kwok, C. Y.; Xu, S.; Kochetkov, I.; Zhou, L.; Nazar, L. F. Highperformance all-solid-state Li2S batteries using an interfacial redox mediator. *Energy Environ. Sci.* **2023**, *16* (2), 610–618.
- (12) Han, F.; Yue, J.; Fan, X.; Gao, T.; Luo, C.; Ma, Z.; Suo, L.; Wang, C. High-Performance All-Solid-State Lithium—Sulfur Battery Enabled by a Mixed-Conductive Li2S Nanocomposite. *Nano Lett.* **2016**, *16* (7), 4521–4527.
- (13) Bandyopadhyay, S.; Nandan, B. A review on design of cathode, anode and solid electrolyte for true all-solid-state lithium sulfur batteries. *Materials Today Energy* **2023**, *31*, No. 101201.
- (14) Du, L.; Wu, R.; Wu, Z.; Huang, H.; Xia, Y.; Gan, Y.; Zhang, W.; Xia, X.; He, X.; Zhang, J. Research progress of all-solid-state lithium—sulfur batteries with sulfide solid electrolytes: materials, interfaces, challenges, and prospects. *Materials Chemistry Frontiers* **2023**, 7 (22), 5760–5785.
- (15) Tan, D. H. S.; Wu, E. A.; Nguyen, H.; Chen, Z.; Marple, M. A. T.; Doux, J.-M.; Wang, X.; Yang, H.; Banerjee, A.; Meng, Y. S. Elucidating Reversible Electrochemical Redox of Li6PSSCl Solid Electrolyte. *ACS Energy Letters* **2019**, *4* (10), 2418–2427.
- (16) Schwietert, T. K.; Arszelewska, V. A.; Wang, C.; Yu, C.; Vasileiadis, A.; de Klerk, N. J. J.; Hageman, J.; Hupfer, T.; Kerkamm, I.; Xu, Y.; van der Maas, E.; Kelder, E. M.; Ganapathy, S.; Wagemaker, M. Clarifying the relationship between redox activity and electrochemical stability in solid electrolytes. *Nat. Mater.* **2020**, *19* (4), 428–435.
- (17) Zhu, Y.; He, X.; Mo, Y. Origin of Outstanding Stability in the Lithium Solid Electrolyte Materials: Insights from Thermodynamic Analyses Based on First-Principles Calculations. *ACS Appl. Mater. Interfaces* **2015**, 7 (42), 23685–23693.
- (18) Sun, X.; Cao, D.; Wang, Y.; Ji, T.; Liang, W.; Zhu, H. All-Solid-State Li—S Batteries Enhanced by Interface Stabilization and Reaction Kinetics Promotion through 2D Transition Metal Sulfides. *Adv. Mater. Interfaces* **2022**, *9* (20), No. 2200539.
- (19) Wang, D.; Jhang, L.-J.; Kou, R.; Liao, M.; Zheng, S.; Jiang, H.; Shi, P.; Li, G.-X.; Meng, K.; Wang, D. Realizing high-capacity all-solid-state lithium-sulfur batteries using a low-density inorganic solid-state electrolyte. *Nat. Commun.* **2023**, *14* (1), 1895.
- (20) Sun, X.; Li, Q.; Cao, D.; Wang, Y.; Anderson, A.; Zhu, H. High Surface Area N-Doped Carbon Fibers with Accessible Reaction Sites for All-Solid-State Lithium-Sulfur Batteries. *Small* **2022**, *18* (6), No. 2105678.
- (21) Zheng, G.; Zhang, Q.; Cha, J. J.; Yang, Y.; Li, W.; Seh, Z. W.; Cui, Y. Amphiphilic Surface Modification of Hollow Carbon Nanofibers for Improved Cycle Life of Lithium Sulfur Batteries. *Nano Lett.* **2013**, *13* (3), 1265–1270.
- (22) Zhang, Q.; Wang, Y.; Seh, Z. W.; Fu, Z.; Zhang, R.; Cui, Y. Understanding the Anchoring Effect of Two-Dimensional Layered Materials for Lithium–Sulfur Batteries. *Nano Lett.* **2015**, *15* (6), 3780–3786.
- (23) Nagao, M.; Imade, Y.; Narisawa, H.; Kobayashi, T.; Watanabe, R.; Yokoi, T.; Tatsumi, T.; Kanno, R. All-solid-state Li-sulfur batteries with mesoporous electrode and thio-LISICON solid electrolyte. *J. Power Sources* **2013**, 222, 237–242.
- (24) Zhang, Q.; Huang, N.; Huang, Z.; Cai, L.; Wu, J.; Yao, X. CNTs@S composite as cathode for all-solid-state lithium-sulfur batteries with ultralong cycle life. *Journal of Energy Chemistry* **2020**, 40, 151–155.
- (25) Lee, B.-J.; Zhao, C.; Yu, J.-H.; Kang, T.-H.; Park, H.-Y.; Kang, J.; Jung, Y.; Liu, X.; Li, T.; Xu, W.; Zuo, X.-B.; Xu, G.-L.; Amine, K.;

- Yu, J.-S. Development of high-energy non-aqueous lithium-sulfur batteries via redox-active interlayer strategy. *Nat. Commun.* **2022**, *13* (1), 4629.
- (26) Lee, B.-J.; Kang, T.-H.; Lee, H.-Y.; Samdani, J. S.; Jung, Y.; Zhang, C.; Yu, Z.; Xu, G.-L.; Cheng, L.; Byun, S.; Lee, Y. M.; Amine, K.; Yu, J.-S. Revisiting the Role of Conductivity and Polarity of Host Materials for Long-Life Lithium—Sulfur Battery. *Adv. Energy Mater.* **2020**, *10* (22), No. 1903934.
- (27) Li, Z.; Zhang, J.; Guan, B.; Wang, D.; Liu, L.-M.; Lou, X. W. A sulfur host based on titanium monoxide@carbon hollow spheres for advanced lithium—sulfur batteries. *Nat. Commun.* **2016**, *7* (1), No. 13065.
- (28) Li, S.; Zhang, W.; Zheng, J.; Lv, M.; Song, H.; Du, L. Inhibition of Polysulfide Shuttles in Li–S Batteries: Modified Separators and Solid-State Electrolytes. *Adv. Energy Mater.* **2021**, *11* (2), No. 2000779.
- (29) Zheng, Y.; Yi, Y.; Fan, M.; Liu, H.; Li, X.; Zhang, R.; Li, M.; Qiao, Z.-A. A high-entropy metal oxide as chemical anchor of polysulfide for lithium-sulfur batteries. *Energy Storage Materials* **2019**, 23, 678–683.
- (30) Liu, X.; Huang, J.-Q.; Zhang, Q.; Mai, L. Nanostructured Metal Oxides and Sulfides for Lithium–Sulfur Batteries. *Adv. Mater.* **2017**, 29 (20), No. 1601759.
- (31) Zhu, Y.; Wang, S.; Miao, Z.; Liu, Y.; Chou, S.-L. Novel Non-Carbon Sulfur Hosts Based on Strong Chemisorption for Lithium—Sulfur Batteries. *Small* **2018**, *14* (40), No. 1801987.
- (32) Liu, T.; Zhang, Y.; Li, C.-H.; Marquez, M. D.; Tran, H.-V.; Robles Hernández, F. C.; Yao, Y.; Lee, T. R. Semihollow Core—Shell Nanoparticles with Porous SiO2 Shells Encapsulating Elemental Sulfur for Lithium—Sulfur Batteries. ACS Appl. Mater. Interfaces 2020, 12 (42), 47368—47376.
- (33) Lee, B.-J.; Park, H.-Y.; Yang, D.-S.; Kang, T.-H.; Hwang, S.; Yu, J.-S. Mesopore Channel Length Control in Ordered Mesoporous Carbon Hosts for High Performance Lithium-Sulfur Batteries. *J. Electrochem. Soc.* **2019**, *166* (3), A5244.
- (34) Yang, D.-S.; Bhattacharjya, D.; Song, M. Y.; Yu, J.-S. Highly efficient metal-free phosphorus-doped platelet ordered mesoporous carbon for electrocatalytic oxygen reduction. *Carbon* **2014**, *67*, 736–743
- (35) Rajan, A. S.; Sampath, S.; Shukla, A. K. An in situ carbongrafted alkaline iron electrode for iron-based accumulators. *Energy Environ. Sci.* **2014**, *7* (3), 1110–1116.
- (36) Deshmukh, P.; Bhatt, J.; Peshwe, D.; Pathak, S. Determination of Silica Activity Index and XRD, SEM and EDS Studies of Amorphous SiO2 Extracted from Rice Husk Ash. *Transactions of the Indian Institute of Metals* **2012**, 65 (1), 63–70.
- (37) Maria Chong, A. S.; Zhao, X. S. Functionalization of SBA-15 with APTES and Characterization of Functionalized Materials. *J. Phys. Chem. B* **2003**, *107* (46), 12650–12657.
- (38) Major, G. H.; Pinder, J. W.; Austin, D. E.; Baer, D. R.; Castle, S. L.; Čechal, J.; Clark, B. M.; Cohen, H.; Counsell, J.; Herrera-Gomez, A.; Govindan, P.; Kim, S. H.; Morgan, D. J.; Opila, R. L.; Powell, C. J.; Průša, S.; Roberts, A.; Rocca, M.; Shirahata, N.; Šikola, T.; Smith, E. F.; So, R. C.; Stovall, J. E.; Strunk, J.; Teplyakov, A.; Terry, J.; Weber, S. G.; Linford, M. R. Perspective on improving the quality of surface and material data analysis in the scientific literature with a focus on x-ray photoelectron spectroscopy (XPS). *J. Vac. Sci. Technol., A* 2023, 41 (3), 038501.
- (39) Foix, D.; Gonbeau, D.; Taillades, G.; Pradel, A.; Ribes, M. The structure of ionically conductive chalcogenide glasses: a combined NMR, XPS and ab initio calculation study. *Solid State Sci.* **2001**, 3 (1), 235–243.
- (40) Lai, Y.-H.; Yeh, C.-T.; Lin, Y.-H.; Hung, W.-H. Adsorption and thermal decomposition of H2S on Si(100). *Surf. Sci.* **2002**, *519* (1), 150–156.
- (41) Liang, X.; Garsuch, A.; Nazar, L. F. Sulfur Cathodes Based on Conductive MXene Nanosheets for High-Performance Lithium—Sulfur Batteries. *Angew. Chem., Int. Ed.* **2015**, *54* (13), 3907–3911.

- (42) Pan, H.; Huang, X.; Zhang, R.; Zhang, T.; Chen, Y.; Hoang, T. K. A.; Wen, G. Reduced graphene oxide-encapsulated mesoporous silica as sulfur host for lithium—sulfur battery. *J. Solid State Electrochem.* **2018**, 22 (11), 3557–3568.
- (43) Liu, Y.; Chen, M.; Hu, M.; Gao, Y. f.; Zhang, Y.; Long, D. Insitu anchoring sulfiphilic silica nanoparticles onto macro-mesoporous carbon framework for cost-effective Li-S cathodes. *Chemical Engineering Journal* **2021**, 406, No. 126781.
- (44) Peng, J.; Zheng, X.; Wu, Y.; Li, C.; Lv, Z.; Zheng, C.; Liu, J.; Zhong, H.; Gong, Z.; Yang, Y. Li2S-Based Composite Cathode with in Situ-Generated Li3PS4 Electrolyte on Li2S for Advanced All-Solid-State Lithium—Sulfur Batteries. ACS Appl. Mater. Interfaces 2023, 15 (16), 20191–20199.
- (45) Kim, J. T.; Rao, A.; Nie, H.-Y.; Hu, Y.; Li, W.; Zhao, F.; Deng, S.; Hao, X.; Fu, J.; Luo, J.; Duan, H.; Wang, C.; Singh, C. V.; Sun, X. Manipulating Li2S2/Li2S mixed discharge products of all-solid-state lithium sulfur batteries for improved cycle life. *Nat. Commun.* 2023, 14 (1), 6404.
- (46) Wang, C.; Wu, Y.; Gao, J.; Sun, X.; Zhao, Q.; Si, W.; Zhang, Y.; Wang, K.; Zhao, F.; Ohsaka, T.; Matsumoto, F.; Huang, C.; Wu, J. Synergistic Defect Engineering and Interface Stability of Activated Carbon Nanotubes Enabling Ultralong Lifespan All-Solid-State Lithium—Sulfur Batteries. ACS Appl. Mater. Interfaces 2023, 15 (34), 40496–40507.
- (47) Sung, J.; Kim, S. Y.; Harutyunyan, A.; Amirmaleki, M.; Lee, Y.; Son, Y.; Li, J. Ultra-Thin Lithium Silicide Interlayer for Solid-State Lithium-Metal Batteries. *Adv. Mater.* **2023**, *35* (22), No. 2210835.
- (48) Liu, Y.; Su, H.; Li, M.; Xiang, J.; Wu, X.; Zhong, Y.; Wang, X.; Xia, X.; Gu, C.; Tu, J. In situ formation of a Li3N-rich interface between lithium and argyrodite solid electrolyte enabled by nitrogen doping. *Journal of Materials Chemistry A* **2021**, 9 (23), 13531–13539.
- (49) Dietrich, C.; Koerver, R.; Gaultois, M. W.; Kieslich, G.; Cibin, G.; Janek, J.; Zeier, W. G. Spectroscopic characterization of lithium thiophosphates by XPS and XAS a model to help monitor interfacial reactions in all-solid-state batteries. *Phys. Chem. Chem. Phys.* **2018**, *20* (30), 20088–20095.
- (50) Auvergniot, J.; Cassel, A.; Foix, D.; Viallet, V.; Seznec, V.; Dedryvère, R. Redox activity of argyrodite Li6PSSCl electrolyte in all-solid-state Li-ion battery: An XPS study. *Solid State Ionics* **2017**, *300*, 78–85.